Existence of broad acoustic bandgaps in three-component composite

Shu Zhang and Jianchun Cheng*

State Key Laboratory of Modern Acoustics and Institute of Acoustics, Nanjing University, Nanjing 210093, China

(Received 14 July 2003; revised manuscript received 27 August 2003; published 1 December 2003)

Experimental and theoretical studies of acoustic transmission through a two-dimensional three-component composite composed of a square array of coated cylinders embedded in an epoxy resin are presented in this paper. The coated cylinders consist of steel inner core and rubber coating, which has much smaller wave velocity and mass density than the matrix and inner material. We observed a broad bandgap in the measured power spectrum along the ΓX propagation direction where only the noise level is measured. The two-component counterparts composed of a square array of steel cylinders embedded in an epoxy resin without rubber coating are also studied to investigate the influence of the soft coating on the properties of bandgaps. The transmission spectrum along the ΓM direction is also presented in the paper. The finite-element method has been employed to calculate the transmitted power spectrum, which is in good agreement with the experimental results. The calculated displacement configurations at the frequency inside and out of the bandgaps illustrate the generation mechanism of the gaps.

DOI: 10.1103/PhysRevB.68.245101 PACS number(s): 43.20.+g, 43.40.+s, 46.40.−f

In the last few years, the existence of forbidden gaps in the band structure of acoustic (AC) and elastic (EL) waves propagation in periodic composite materials has received a great deal of attention.[1-6] Acoustic gaps are frequency domains in which propagation of sound and elastic waves is forbidden, which are analogous to photonic bandgaps[7] for electromagnetic waves. The design of broad forbidden gaps in transmission spectrum has been a subject of great interest, which may have many engineering applications. Different geometries of two-dimensional (2D) systems, such as square,[8,9] hexagonal,[10,11] and centered rectangular lattice[12] and boron nitride- (BN-) like structures,[13] have been investigated in search of large gaps. But the early work focuses mainly on two-component systems.[14-17] Recently, the idea of three-component crystal structure has been proposed by Liu *et al.*[18] The localized resonant structure can lead to complete sound attenuation in some frequency intervals, which has spurred a new area of research.[19,20]

In this paper, we present a theoretical and experimental study of the transmission of elastic waves across crystal slabs made up of a square array of coated cylinders embedded in an epoxy matrix with thickness along two different directions of the square Brillouin zone. Hard steel cylinders and elastically soft rubber coating constitute the inclusions. In contrast to the transmission spectrum of the two-component counterparts consisting of a square array of steel cylinders embedded in an epoxy resin, those of the three-component composite show attenuation to noise level intensity in a much larger frequency interval along the ΓX direction. The finite-element (FE) method has been employed for modeling the propagating and scattering of elastic waves across the crystal slab. Comparison of the experimental results with the calculation shows good agreement.

Our experimental setup is based on the well-known ultrasonic transmission technique. A couple of ultrasonic broadband transducers with a central frequency of 1 MHz (Panametrics contact transducers type Videoscan No. V102) were used in the experiment, launching a probing wave signal from the emitter through the composite sample, which is then processed at the receiver. The emitter is centered on the transversal face of the composite and the nearly parallel signal is perpendicular to the cylinders. The emitter was excited with an ultrasonic emission source (Panametrics model 5800PR) producing a short-duration large-amplitude pulse. The signal acquired by the receiver is digitized with a Tektronix digital oscilloscope with real-time fast Fourier transform (FFT) capability to produce the power spectrum.

We have manufactured two three-component and two two-component composite samples of the same physical dimensions, 88 mm×39 mm×50 mm. The thicknesses of the same component samples are along two different directions of the Brillouin zone, respectively, to study the influence of the direction of propagation on the bandgaps. The sample contains 60 inclusions of 5 columns or 59 inclusions of 7

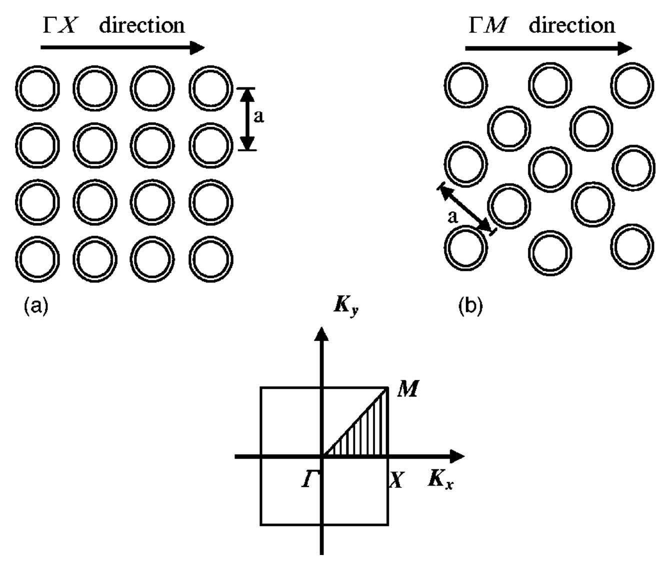

FIG. 1. Two-dimensional cross section of the square arrays of coated cylinders distributed in an epoxy matrix along the (a) ΓX and (b) ΓM directions, respectively. The inset shows the two-dimensional irreducible Brillouin zone of the square array, and $\vec{K}(K_X, K_Y)$ is a two-dimensional wave vector.

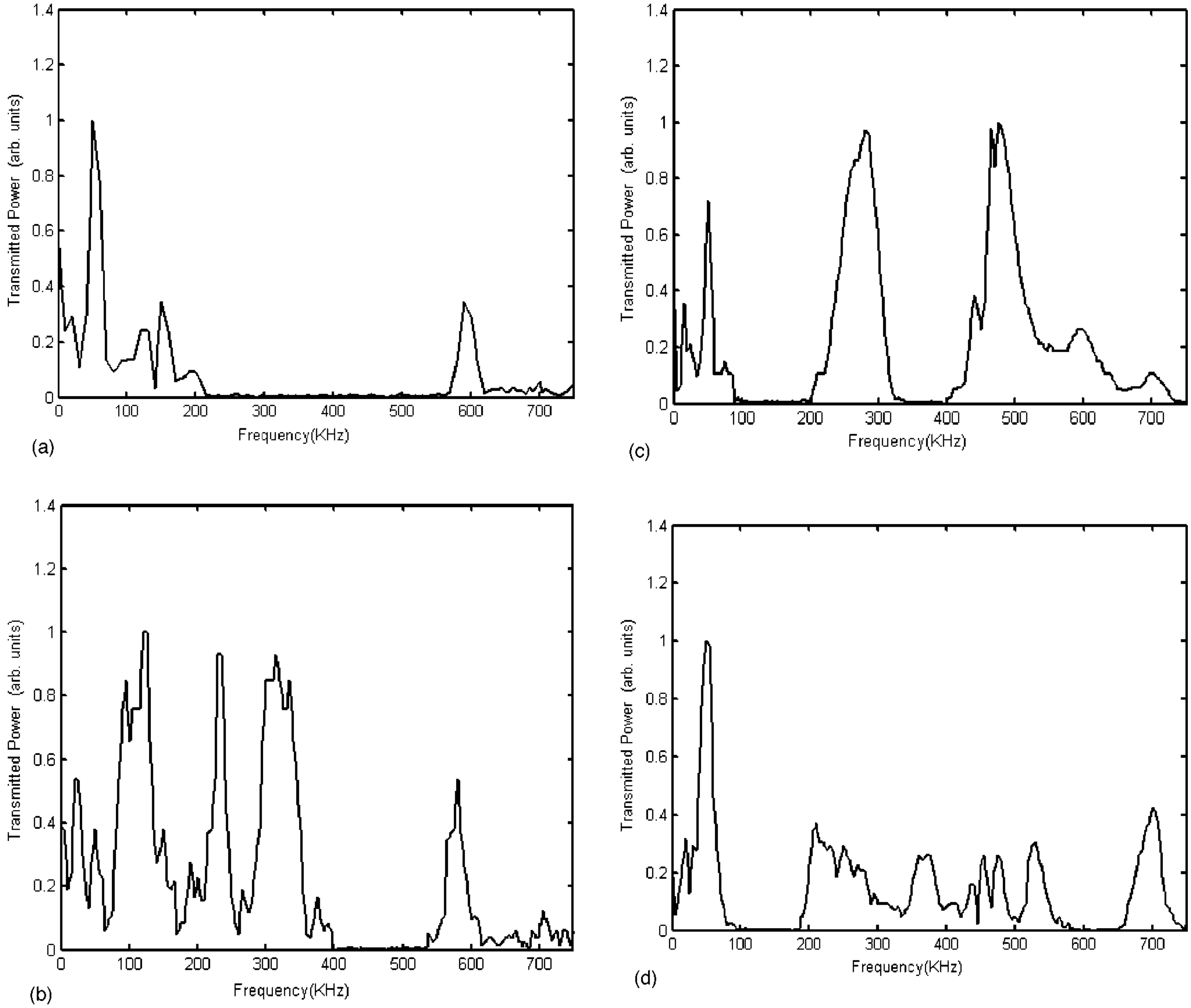

FIG. 2. Experimental transmission spectrum measured perpendicular to the vertical face of the three-component composite samples along (a) the ΓX direction and (b) the ΓM direction and the two-component composite samples along (c) the ΓX direction and (d) the ΓM direction.

columns along the ΓX or ΓM direction, respectively. The lattice constant and filling fraction of the inclusions are equal in all samples. The lattice constant is $a=7$ mm. The steel cylinder has a diameter $d_1=5$ mm in the two-component crystal slab. The diameter of the coated cylinder is $d_2=5$ mm and the core steel cylinder is $d_1=4$ mm. The thickness of the rubber coating is 1 mm. We have illustrated in Fig. 1 the cross section of the specimens.

A broad low transmission intensity appears clearly in the power spectrum of the three-component composite along the ΓX direction as we can see from Fig. 2(a). The gap extends from 220 to 560 kHz followed by a sharp rise in transmission centered at 600 kHz. In Fig. 2(b), one noise-level transmission interval appears clearly from 400 to 530 kHz.

The transmitted spectra of the two-component composite along the ΓX and ΓM directions are illustrated in Figs. 2(c) and 2(d), respectively. Two forbidden gaps are shown clearly in Figs. 2(c) and 2(d), in region of 100–200 kHz and 340–400 kHz in the ΓX direction and 100–190 kHz and 580–650 kHz in the ΓM direction.

From a comparison of Figs. 2(a) and 2(c), we can obtain a much broader forbidden gap when the embedded cylinders are coated with a rubber layer. Because of the same geometry arrangement and equal size of the matrix and inclusions in the three and two-component composite, the elastically soft coating layer is the main reason for the broadening of the band gaps. The coating layer is softer compared with the elastic constant of the matrix and the core material, which meets the condition for local resonance.[19] However, no obvious broadening is observed along the ΓM direction in Fig. 2(b) compared with Fig. 2(d). The difference in the transmitted spectrum of the three-component composite along two directions is a signature that the sample geometry influences the gap properties and that the Bragg mechanism in periodic systems also plays a role in the bandgap generation in the high-frequency range. The three-component samples have a

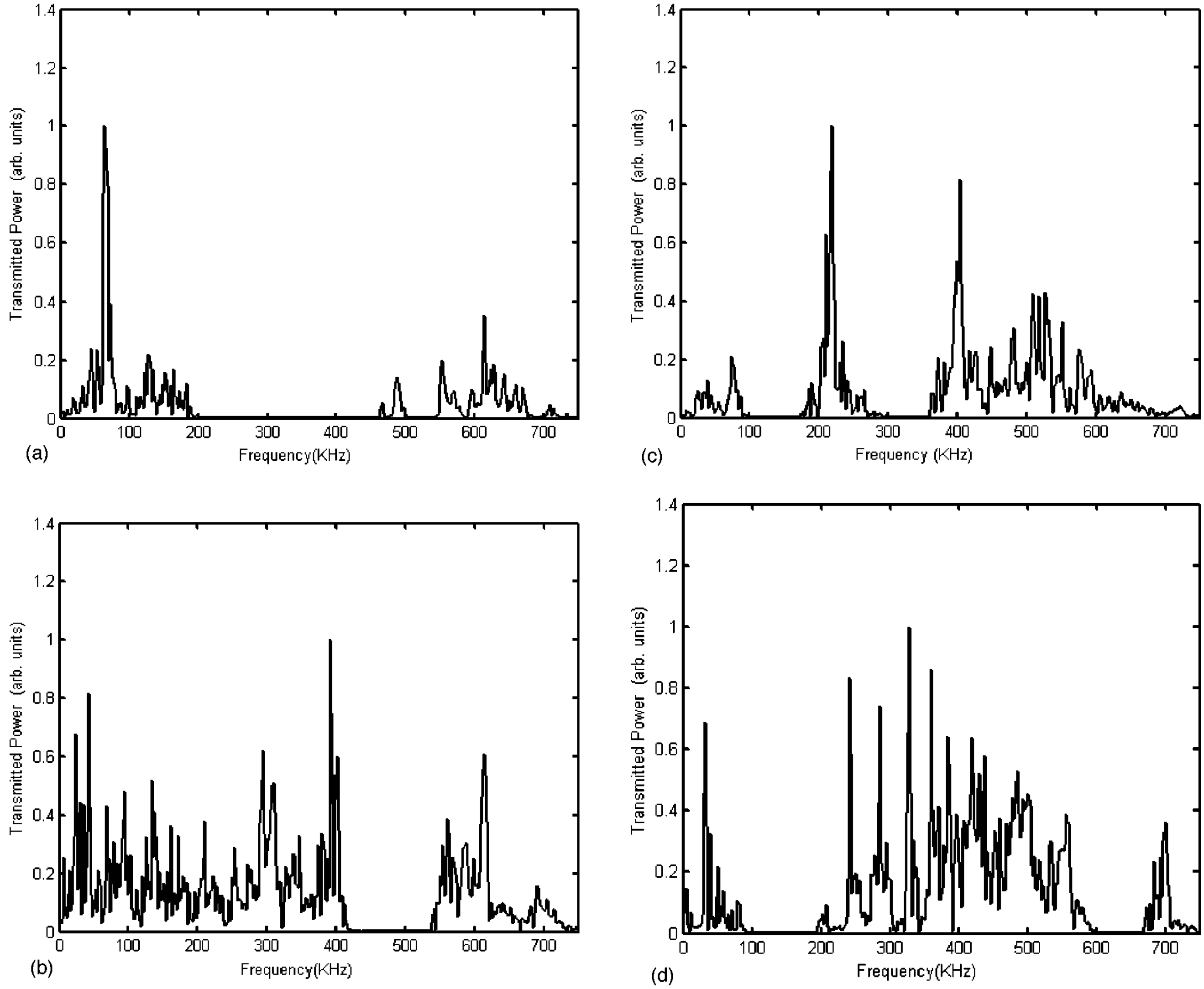

FIG. 3. Theoretical transmission power spectrum computed by the FE method of the three-component composite sample along (a) the ΓX direction, (b) the ΓM direction and the two-component composite sample along (c) the ΓX direction, (d) the ΓM direction.

high concentration of the embedded units with filling fraction of 40% so that the individual resonances couple strongly with each other.[19] The two mechanisms of linear dispersion and resonance of the individual coated cylinder open the forbidden gap.

Theoretical transmission spectra are calculated using the 2D FE method. The FE solution involves the discretization of the domain into a number of elements, approximating the displacement values interior to the elements in terms of its nodal value through the shape functions of the chosen element and the determination of nodal values.[21,22] In this work, the sample size and the scatter arrangement are fixed at the experimental values[23] with the thickness (ΓX or ΓM direction) along the Y direction. A uniform four-node quadrilateral element mesh for spatial discretization is used as recommended for wave propagation problems.[24] The step sizes of temporal and spatial discretization in the finite model are fine enough for the convergence of the numerical results. The transducer is modeled as a traction boundary condition applied for a finite duration. The force is a sinusoidal wave weighted by a Gaussian profile whose spectrum envelope resembles the experimental one. The transmitted longitudinal displacement vector u_y is collected as a function of time at the other side of the model. For a sufficiently large number of these u_y data on the time axis, the displacement fields are Fourier transformed into the frequency space to yield the transmitted power.

The FE calculated transmission spectra of the three-component composite are shown in Figs. 3(a) and 3(b). One broad forbidden gap from 200 to 460 kHz is present in Fig. 3(a) along the ΓX direction. There is another low-transmission region from 500 to 545 kHz. Compared to the experimental spectrum in Fig. 2(a), the peak centered at 490 kHz separates one broad bandgap from 200 to 545 kHz to two bandgaps. Along the ΓM direction, the width of the gap from 420 to 535 kHz in Fig. 3(b) is slightly narrower than the measured one in Fig. 2(b).

Figures 3(c) and 3(d) show the transmission spectrum of the two-component composite sample computed with the FE method along the ΓX and ΓM directions, respectively. The

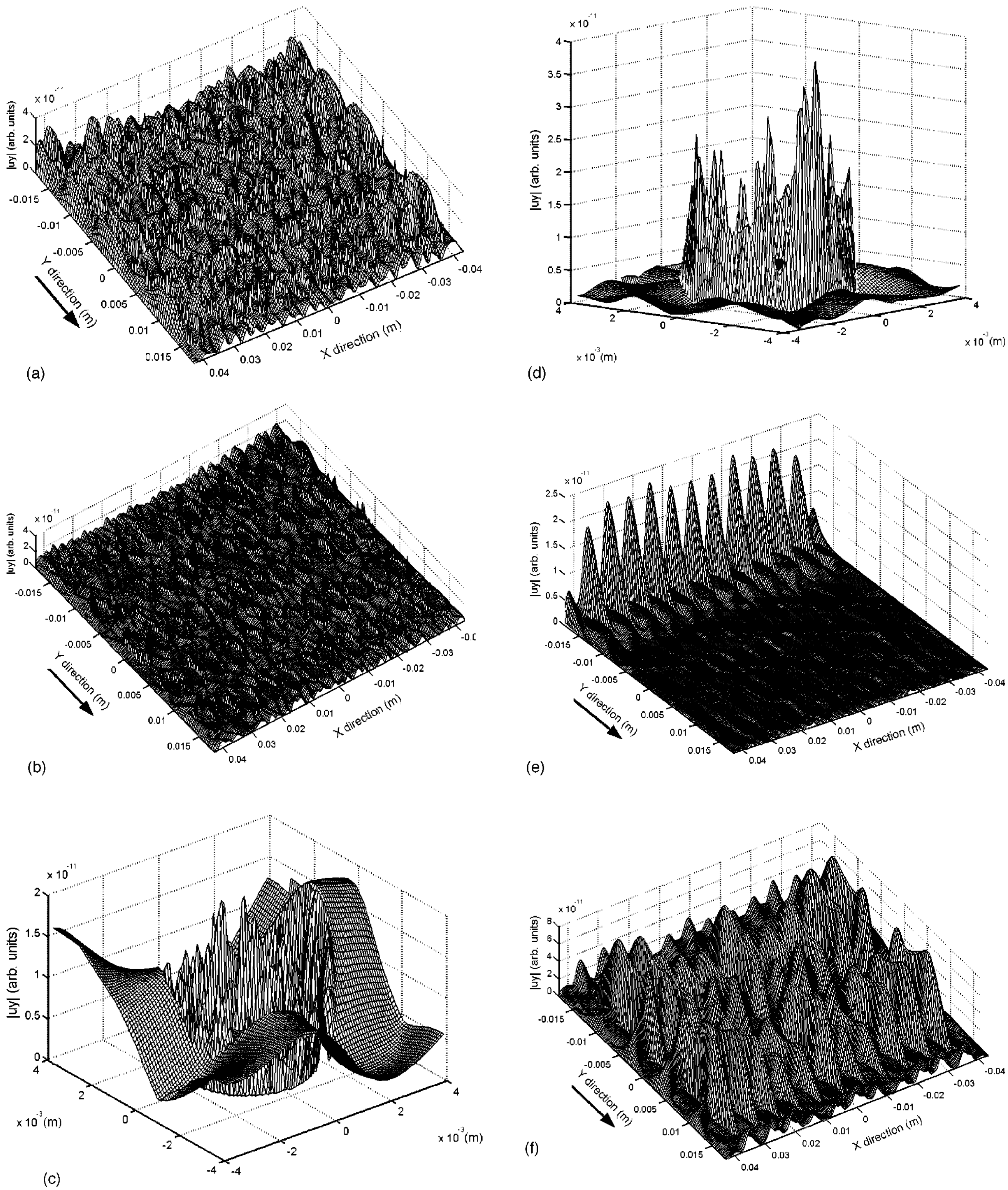

FIG. 4. The longitudinal displacement u_y field output along the ΓX direction of the three-component sample at frequency (a) 150 kHz, (b) 250 kHz and one unit in the three-component composite at (c) 150 kHz, (d) 250 kHz, and the two-component sample at frequency (e) 150 kHz and (f) 250 kHz. The arrows indicate the direction of the incident wave (Y direction).

first well-defined drop in intensity in Fig. 3(c) appears between 100 and 180 kHz, which is in good agreement with the measured one in Fig. 2(c). At the higher-frequency range, the transmission power drops to a noise level from 300 to 350 kHz, which may be compared with the second bandgap in Fig. 2(c). The first low-level transmission interval appears from 100 to 195 kHz in Fig. 3(d) and the second gap from 600 to 670 kHz. One notes that the two bandgaps in the experimental spectrum [see Fig. 2(d)] overlap with the theoretical ones.

Comparison of Figs. 2 and 3 shows good correspondence in the position of the forbidden gaps between the experimental and theoretical transmission spectra. One should note that because the transmitted power is strongly attenuated at the high-frequency range, it is difficult to define precisely the edges of the region with the noise level transmission. However, some discrepancies remain when considering the exact width and edges of the bandgaps. One possible reason for these discrepancies is the difference between the computation model and the samples measured in the experiment. The computation is performed on a 2D model assuming the model is very thick relative to its lateral dimensions, while the size along the cylinder axis of the samples in the experiment is comparable to their lateral size along the propagation direction. The less agreement of the bandgap position in the higher-frequency than in the lower-frequency range is a signature of the greater influences resulting from the small imperfections in the experimental samples on shorter wavelengths. The absorption and viscous-loss effect in the experiment that is not included in the calculation also lead to the difference between the experimental and theoretical results. And this effect is more serious in the higher-frequency domain. The external loading in the calculation may not coincide exactly with the signal emitted by the transmitting transducer in the spectrum envelop and the emitted signal is not a true plane wave in the experiment along the incident direction as the theoretical calculation assumes.

We have also investigated the displacement field output of the calculation model. By comparing the longitudinal displacement u_y field output along the ΓX direction at frequencies inside and outside the bandgaps, we can investigate the generation mechanism for the bandgaps. The unit in the z axis is arbitrary for absolute values of the displacement u_y. All field outputs in Fig. 4 are results of the same calculation unit and same loading conditions. The displacement fields in the three-component composite at frequency 150 kHz out of the bandgap and 250 kHz inside the gap are presented in Figs. 4(a) and 4(b), respectively. Figures 4(c) and 4(d) show only one unit in Figs. 4(a) and 4(b), respectively. Outside the bandgaps the field is uniformly distributed and we can see an obvious extended wave shape as shown in Figs. 4(a) and 4(c). Large transmitted power can be observed in the receiving side of the epoxy host. Inside the bandgap, the local resonance leads to a very larger displacement in the rubber than that in the epoxy resin as we can see from Figs. 4(b) and 4(d). The greater part of the strength is localized in the rubber coating and little is transmitted in the epoxy host. Comparing the displacements in the epoxy host in Figs. 4(c) and 4(d), we can see those outside the bandgap in Fig. 4(c) are approximately one order of magnitude larger than those inside the band gap in Fig. 4(d). In this way, the bandgap is observed for small transmitted power on the receiving side of the epoxy resin.

Figures 4(e) and 4(f) show the displacement fields of the two-component composite at frequency 150 kHz inside the gap and 250 kHz outside the gap frequency. The displacement amplitude in Fig. 4(e) becomes very small after propagating across one layer of the steel cylinders because the almost full reflection resulting from Bragg scattering prevents the strength from transmitting across just one layer of the steel cylinders. But the wave outside the bandgap can cross the composite without big reflections as we can see from Fig. 4(f).

From comparison of Fig. 4(b) with Fig. 4(e), we observed an absolutely different representation of the displacement u_y in the bandgap frequency. In the three-component composite, the localized resonance in the soft rubber coating is the dominant mechanism for the bandgaps, while Bragg scattering is the only reason for gap generation in the two-component composite.

In summary, we have studied the band structure in the 2D three-component system. The width and frequency domains of the theoretical band gaps are comparable to those of the measured one. Both results proved unambiguously the existence of a much broader bandgap in the three-component crystal slab along the ΓX direction than those in the two-component one, which has equal physical size, filling fraction, and the same geometry of inclusions. In light of the agreement between the measured and calculated gaps, we believe that the use of an elastically soft coating layer can be a way to broaden the forbidden gap.

This work was supported by the Excellent Youth Science Foundation of China, under Grant No. 10125417.

*Author to whom correspondence should be addressed.

[1] M. M. Sigalas and E. N. Economou, Solid State Commun. **86**, 141 (1993).

[2] M. S. Kushwaha, P. Halevi, and G. Martinez, Phys. Rev. B **49**, 2313 (1994).

[3] F. R. Montero de Espinosa, E. Jiménez, and M. Torres, Phys. Rev. Lett. **80**, 1208 (1998).

[4] M. Torres, F. R. Montero de Espinosa, D. Garcia-Pablos, and N. Garcia, Phys. Rev. Lett. **82**, 3054 (1999).

[5] Ph. Lambin, A. Khelif, J. O. Vasseur, L. Dobrzynski, and B. Djafari-Rouhani, Phys. Rev. E **63**, 066605 (2001).

[6] R. Mártinez-Sala, J. Sancho, J. V. Sánchez-Pérez, J. Linares, and F. Meseguer, Nature (London) **378**, 241 (1995).

[7] S. John, Phys. Rev. Lett. **58**, 2486 (1987).

[8] J. O. Vasseur, B. Djafari-Rouhani, L. Dobrzynski, M. S. Kushwaha, and P. Halevi, J. Phys.: Condens. Matter **6**, 8759 (1994).

[9] M. S. Kushwaha, P. Halevi, L. Dobrzynski, and B. Djafari-Rouhani, Phys. Rev. Lett. **71**, 2022 (1993).

[10] M. M. Sigalas and E. N. Economou, J. Appl. Phys. **75**, 2845 (1994).

[11] M. S. Kushwaha and P. Halevi, Appl. Phys. Lett. **64**, 1085 (1994).

[12] J. O. Vasseur, P. A. Deymier, G. Frantziskonis, G. Hong, B. Djafari-Rouhani, and L. Dobrzynski, J. Phys.: Condens. Matter **10**, 6051 (1998).

[13] J. O. Vasseur, B. Djafari-Rouhani, L. Dobrzynski, and P. A. Deymier, J. Phys.: Condens. Matter **9**, 7327 (1997).

[14] E. N. Economou and M. M. Sigalas, J. Acoust. Soc. Am. **95**, 1734 (1994).

[15] J. V. Sánchez-Pérez, D. Caballero, R. Mártinez-Sala, C. Rubio, J. Sánchez-Dehesa, F. Meseguer, J. Linares, and F. Gálvez, Phys. Rev. Lett. **80**, 5325 (1998).

[16] D. García-Pablos, M. Sigalas, F. R. Montero de Espinosa, M. Torres, M. Kafesaki, and N. Garcia, Phys. Rev. Lett. **84**, 4349 (2000).

[17] J. O. Vasseur, P. A. Deymier, B. Chenni, B. Djafari-Rouhani, L. Dobrzynski, and D. Prevost, Phys. Rev. Lett. **86**, 3012 (2001).

[18] Z. Liu, X. Zhang, Y. Mao, Y. Y. Zhu, Z. Yang, C. T. Chan, and PingSheng, Science **289**, 1734 (2000).

[19] Z. Liu, C. T. Chan, and PingSheng, Phys. Rev. B **65**, 165116 (2002).

[20] C. Goffaux, J. Sánchez-Dehesa, A. Levy Yeyati, Ph. Lambin, A. Khelif, J. O. Vasseur, and B. Djafari-Rouhani, Phys. Rev. Lett. **88**, 225502 (2002).

[21] K. J. Bathe, *Finite Element Procedures* (Prentice-Hall, New York, 1995).

[22] O. C. Zienkiewicz, *The Finite Element Method* (McGraw-Hill, London, 1977).

[23] The parameters used in the calculation are $\rho=7.9\times10^3$ kg/m^3, $E=2.138\times10^{11}$ N/m^2, $\sigma=0.29$ for steel, $\rho=1.18\times10^3$ kg/m^3, $E=4.35\times10^9$ N/m^2, $\sigma=0.368$ for epoxy, $\rho=1.3\times10^3$ kg/m^3, $E=1.18\times10^5$ N/m^2, $\sigma=0.469$ for rubber, where ρ, E, and σ are the density, Young's modulus, and Poisson's ratio, respectively.

[24] K. J. Bathe, *Finite Element Procedures in Engineering Analysis* (Prentice-Hall, New York, 1982).